ELSEVIER

Catalysis Today 83 (2003) 115–129

CATALYSIS TODAY

www.elsevier.com/locate/cattod

Kinetic measurements of CH_4 combustion over a 10% PdO/ZrO_2 catalyst using an annular flow microreactor

W. Ibashi[1], G. Groppi*, P. Forzatti

Dipartimento di Chimica Materiali e Ingegneria Chimica "G. Natta", Politecnico di Milano—CMIC, Piazza Leonardo da Vinci 32, 20133 Milan, Italy

Received 1 May 2002; received in revised form 20 November 2002; accepted 18 March 2003

Abstract

A kinetic study on CH_4 combustion over a PdO/ZrO_2 (10%, w/w) catalyst has been performed in a temperature range between 400 and 550 °C by means of an annular catalytic microreactor.

The role of mass transfer phenomena including diffusion in the catalyst pore, gas–solid diffusion and axial diffusion in the gas phase, has been preliminary addressed by means of mathematical modeling. Simulation results have pointed out the key role of internal diffusion showing that thicknesses of the active catalyst layer as thin as 10–15 μm are required to minimize the impact of mass transfer limitations. The thermal behavior of the reactor has been also addressed by means of catalytic combustion tests with CH_4 and $CO–H_2$ mixtures as fuels. The results have demonstrated the possibility to obtain nearly isothermal temperature profiles under severe conditions (up to 3% of CH_4) thanks to effective dissipation of reaction heat by radiation from the catalyst outer skin.

Finally the effect of reactants (CH_4 and O_2) and products (H_2O and CO_2) on CH_4 combustion rate has been addressed. The results have shown that both H_2O and CO_2 markedly inhibit the reaction up to 550 °C. The data have been fitted by the following simple power law expression $r = k_r P_{CH_4} P_{H_2O}^{-0.32} P_{CO_2}^{-0.25}$ with an apparent activation energy of 108 kJ/mol.

Evidences have been found and discussed indicating a key role of the support on the extent of such inhibition effects.

Keywords: CH_4 combustion kinetics; PdO/ZrO_2 catalyst; Annular catalytic reactor

1. Introduction

PdO supported systems are the catalyst of choice in catalytic combustors for natural gas fuelled gas turbines with ultra-low emissions of NO_x, CO and unburned hydrocarbons [1]. This is due to the following key properties: (i) maximum activity in CH_4 combustion [2]; (ii) negligible volatility of all the relevant Pd species; (iii) "chemical thermostat" ability associated with reversible PdO/Pd transformation. Despite their importance few kinetic data are available in relevant temperature range to gas turbine applications (>400 °C) due to the difficulties associated with diffusional and pressure drop limitations in the presence of a very exothermic reaction (CH_4 combustion, $\Delta H_r = 803.7$ kJ/mol) to be performed over

* Corresponding author. Tel.: +39-02-23993258; fax: +39-02-70638173.
E-mail address: gianpiero.groppi@polimi.it (G. Groppi).
[1] Present address: Environmental Process Development Department, Industrial Machine and Plant Development Center, Ishikawajima-Harima Heavy Industries Co., Ltd., Yokohama, Japan.

0920-5861/$ – see front matter © 2003 Elsevier B.V. All rights reserved.
doi:10.1016/S0920-5861(03)00221-9

Nomenclature

A_{axial}	cross-sectional area of the wall of the ceramic tube (m^2)
A_{radial}	wetted surface of the catalyst layer (m^2)
C_f	concentration of *f*-species (mol/m^3)
$d_h = 2[r_0 - (r_i + \delta_w)]$	hydraulic diameter (m)
$D_{ea,f}$	effective axial diffusion of *f*-species (m^2/s)
$D_{ei,f}$	effective intraporous diffusion coefficient of *f*-species (m^2/s)
$D_{m,f}$	molecular diffusion coefficient of *f*-species (m^2/s)
F_t	total molar flow rate (mol/s)
ΔH_f	molar combustion enthalpy of *f*-species (kJ/mol)
$K_{g,f} = D_{m,f}Sh/d_h$	gas–solid mass transfer coefficient of *f*-species (m/s)
K_{H_2O}	adsorption constant of H_2O (m^3/mol)
K_r	reaction rate constant (1/s)
L	catalyst length (m)
n	coordinate in catalyst (m)
r_i	external diameter of the ceramic tube (m)
r_0	internal diameter of the quartz tube (m)
$R_{w,f}$	reaction rate of *f*-species ($mol/m^3/s$)
$Re = \rho_g u d_h/\mu_g$	Reynolds number
$Sc_f = \mu_g/\rho_g D_{m,f}$	Schmidt number of *f*-species
$Sh_f = K_{g,f}d_h/D_{m,f}$	Sherwood number of *f*-species
u	axial velocity (m/s)
X_f	conversion of *f*-species
y_f	molar ratio of *f*-species
z	axial coordinate (m)

Greek symbol

δ_A	height of the annular chamber (m)
δ_w	catalyst wall thickness (m)
μ	viscosity (kg/m/s)
ν_f	stoichiometric coefficient of *f*-species in reaction
ρ	density (kg/m^3)

Subscripts and Superscripts

g	gas phase
0	inlet condition
w	catalyst layer

very active highly loaded PdO catalysts at extremely high GHSV ($>10^6\ h^{-1}$).

To overcome these problems McCarty [3] proposed an annular reactor in which a ceramic tube coated with a thin catalyst layer is placed coaxially in a quartz tube forming an annular chamber where the reacting gas flows. Thanks to the straightforward flow pattern and the very small catalyst load, it is possible to perform the activity measurements at very high GHSV (10^6–$10^7\ h^{-1}$) with negligible pressure drops. Therefore partial conversion could be obtained even in the presence of very fast reactions such as high temperature CH_4 combustion over palladium catalysts. An additional feature of the reactor is the well

defined structured geometry which allows for careful assessment of diffusional effects. This advantage was pointed out in previous papers [4,5] where preliminary design of the annular reactor was performed by mathematical modeling aimed at the definition of a reactor configuration able to minimize the impact of diffusional limitations. Simulation results for a $PdO/\gamma\text{-}Al_2O_3$ catalyst evidenced the critical role of internal mass transfer limitations which could be suppressed to a reasonable extent only by thinning the catalyst layer down to 10 μm.

In this paper a similar modeling analysis was performed for a PdO/ZrO_2 (10%, w/w of Pd) catalyst. Systems with high Pd loading supported on ZrO_2 have been reported as the most effective catalysts in catalytic combustors for gas turbines [6]. Besides the morphology ZrO_2 with low porosity and low surface area is quite different from that of $\gamma\text{-}Al_2O_3$, thus deserving a specific modeling analysis. Along the lines provided by mathematical model design an annular flow microreactor was prepared by wash-coating deposition of a thin layer of PdO/ZrO_2. The results of a kinetic study performed over such a reactor, including effects of reactants (CH_4 and O_2) and products (H_2O and CO_2) on CH_4 combustion rate in a 400–550 °C temperature range, are here reported and discussed. Data on the thermal behavior of the reactor were also collected to analyze the prevailing heat dissipation mechanisms.

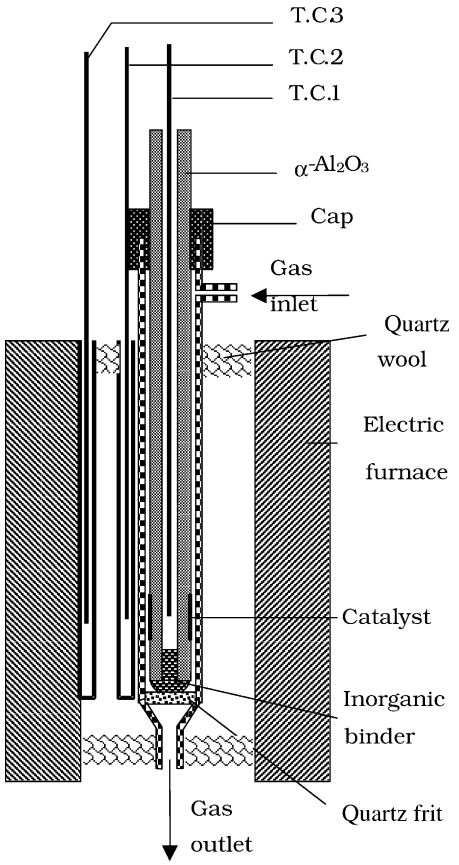

Fig. 1. Schematic illustration of the annular reactor.

2. Mathematical model analysis

A schematic sketch of the annular reactor used in this work is reported in Fig. 1. The reactor consists of an internal $\alpha\text{-}Al_2O_3$ ceramic tube coaxially inserted into an external quartz tube and is vertically placed in an electric oven. The gas flows downwards in the annulus between the ceramic and the quartz tubes. The PdO/ZrO_2 catalyst is deposited on the external surface of the ceramic tube, near the bottom of the annular duct to enhance pre-heating of the gas stream. The bottom of the ceramic tube is sealed with thermal cement to avoid gas leakage.

The impact of diffusional phenomena on kinetic measurements of very fast reactions was preliminary analyzed along the lines proposed in a previous work [4].

Two types of models, A and B, were considered. In model A mass transfer effects associated with external gas–solid diffusion, internal diffusion in the porous catalyst layer, axial diffusion in the gas phase were included. In model B all the mass transfer limitations were neglected.

Model A provides a one-dimensional description for the gas phase and a two-dimensional one for the catalyst layer under the following assumptions: (i) fully developed laminar flow in the annular chamber at the catalyst inlet; (ii) steady state and isothermal conditions; (iii) parallel plate configuration which can be applied in view of the much smaller catalyst thickness compared to the radius of the tube ($r_i/\delta_w > 50$), and (iv) negligible pressure drop. The model consists of following mass balance equations and boundary conditions.

Mass balance of *f*-species (CH_4, H_2O and CO_2) in gas phase:

$$-u\frac{\partial C_{f,\mathrm{g}}}{\partial z} + (D_{\mathrm{m},f} + D_{\mathrm{ea},f})\frac{\partial^2 C_{f,\mathrm{g}}}{\partial z^2} - \frac{4}{d_\mathrm{h}}\frac{r_\mathrm{i} + \delta_\mathrm{w}}{r_0 + (r_\mathrm{i} + \delta_\mathrm{w})}K_{\mathrm{g},f}(C_{f,\mathrm{g}} - C_{f,\mathrm{w}}) = 0 \quad (1)$$

Mass balance of *f*-species (CH_4, H_2O and CO_2) in the catalyst layer:

$$D_{\mathrm{ei},f}\frac{\partial^2 C_{f,\mathrm{w}}}{\partial n^2} + R_{f,\mathrm{w}} = 0 \quad (2)$$

Boundary conditions at inlet ($z = 0$) and outlet ($z = L$) of the catalyst layer:

$$u(C_{f,\mathrm{g}} - C^0_{f,\mathrm{g}}) = (D_{\mathrm{m},f} + D_{\mathrm{ea},f})\frac{\partial C_{f,\mathrm{g}}}{\partial z} \quad \text{at } z = 0,$$

$$\frac{\partial C_{f,\mathrm{g}}}{\partial z} = 0 \quad \text{at } z = L \quad (3)$$

Boundary conditions at the interface ($n = 0$) between the catalyst layer and the external surface of the tube and at the interface ($n = \delta_\mathrm{w}$) between gas and the surface of the catalyst layer are

$$\frac{\partial C_{f,\mathrm{w}}}{\partial n} = 0 \quad \text{at } n = 0,$$

$$D_{\mathrm{ei},f}\frac{\partial C_{f,\mathrm{w}}}{\partial n} = K_{\mathrm{g},f}(C_{f,\mathrm{g}} - C_{f,\mathrm{w}}) \quad \text{at } n = \delta_\mathrm{w} \quad (4)$$

Sherwood number account for entrance effect and is given by

$$Sh_f = Sh_\infty + 6.874\left(\frac{1000z}{d_\mathrm{h}\,Re\,Sc_f}\right)^{-0.488} \times \exp\left(-\frac{57.2z}{d_\mathrm{h}\,Re\,Sc_f}\right) \quad (5)$$

Effective axial dispersion is given by

$$D_{\mathrm{ea},f} = \frac{u^2 d_\mathrm{h}^2}{192 D_{\mathrm{m},f}} \quad (6)$$

The following rate equation was considered

$$R_{\mathrm{w},f} = \nu_f\left(\frac{K_\mathrm{r}C_{\mathrm{CH_4}}}{1 + K_{\mathrm{H_2O}}C_{\mathrm{H_2O}}}\right) \quad (7)$$

which takes into account the effect of water inhibition that was reported by several authors [4,5,7–9]. This was required in order to properly assess the impact of the different mass transfer effects which can significantly change in the presence of product inhibition. Kinetic parameters reported in Table 1 were set in order to be representative of a very active catalyst able to provide high conversion (about 60%) at 550 °C with extremely high GHSV ($2 \times 10^6\,\mathrm{h}^{-1}$).

The governing PDEs was numerically solved according to the following procedure. Orthogonal collocations on finite elements method and orthogonal collocations method were applied to variable discretization for the *z*-coordinate and for the *n*-coordinate, respectively. The resulting AEs was solved by a continuation method. Seven elements for *z*-coordinate and four internal collocation points for *n*-coordinate occurred to achieve the numerical convergence.

In model B all of the diffusional limitations were neglected and a one-dimensional pseudo-homogenous reactor was assumed. Accordingly the model consists of the following mass balance equation and inlet condition:

$$u\frac{\mathrm{d}C_f}{\mathrm{d}z} + \frac{(r_\mathrm{i} + \delta_\mathrm{w})^2 - r_\mathrm{i}^2}{r_0^2 - (r_\mathrm{i} + \delta_\mathrm{w})^2}R_f^{\mathrm{eff}} = 0 \quad (8)$$

$$C_f = C_f^0 \quad \text{at } z = 0 \quad (9)$$

with

$$R_f^{\mathrm{eff}} = \nu_f\left(\frac{K_\mathrm{r}^{\mathrm{eff}}C_{\mathrm{CH_4}}}{1 + K_{\mathrm{H_2O}}C_{\mathrm{H_2O}}}\right) \quad (10)$$

The governing ODE was solved by LSODI library routine.

The impact of diffusional limitations was evaluated by calculation of the internal and the overall effectiveness factor as a function of the reactor geometry.

η_{int} gives the extent of internal diffusion limitation and was calculated by Eq. (11) using concentration field for each gas component obtained from model A:

$$\eta_{\mathrm{int}} = \frac{1}{L}\int_0^L\left[\frac{1}{\delta_\mathrm{w}R_\mathrm{w}(z,0)}\int_0^{\delta_\mathrm{w}}R_\mathrm{w}(z,n)\,\mathrm{d}n\right]\mathrm{d}z \quad (11)$$

η_{total} was calculated from the equation given below:

$$\eta_{\mathrm{total}} = \frac{K_\mathrm{r}^{\mathrm{eff}}}{K_\mathrm{r}} \quad (12)$$

In Eq. (12) K_r is the actual rate constant in model A and $K_\mathrm{r}^{\mathrm{eff}}$ is the rate constant in Eq. (10) of model B calculated by regression in order to fit the outlet concentration derived from model A. Accordingly η_{total}

Table 1
Simulation parameters (Sh_∞: 5.385)

Gas properties		
C_{tot} (mol/m^3)	14.82	
$D^{He}_{m,f}$ (m^2/s)	3.048×10^{-4} (CH_4)	3.451×10^{-4} (H_2O)
$D^{N_2}_{m,f}$ (m^2/s)	1.287×10^{-4} (CH_4)	1.352×10^{-4} (H_2O)
Catalyst morphology		
Pore 1	$\varepsilon = 0.096$	$r_p = 28$ nm
Pore 2	$\varepsilon = 0.13$	$r_p = 64$ nm
$D^{He}_{e,f}$ (m^2/s)	9.255×10^{-7} (CH_4)	8.887×10^{-7} (H_2O)
$D^{N_2}_{e,f}$ (m^2/s)	8.076×10^{-7} (CH_4)	8.266×10^{-7} (H_2O)
Operating conditions		
Flow rate (m^3/s at STP)	1.67×10^{-6}	
T (K)	823	
P (bar)	1	
% O_2 (v/v)	20	
% CH_4 (v/v)	0.75	
Carrier (He/N_2)	Balance	
Kinetics		
K_r (s^{-1})	2.326×10^3	
K_{H_2O} (m^3/mol)	4.151	
Geometry		
L (m)	1.0×10^{-2}	
r_0 (m)	3.50×10^{-3}	

includes the limitations associated with all the mass transfer phenomena and it is always ≤ 1: mass transfer limitations are negligible if η_{total} is close to 1.

Simulations were performed for the set of parameter values reported in Table 1, which corresponds to high temperature (550 °C) combustion of CH_4 over a very active Pd based catalyst. The bimodal pore distribution consisting of mesopores (mean radius: 28 nm; porosity: 0.096) and macropores (mean radius: 65 nm; porosity: 0.13) considered for the PdO/ZrO_2 catalyst layer was derived from pore size measurements obtained upon preliminary deposition tests.

Fig. 2 shows the simulated contours of η_{total} (Fig. 2a and d), η_{int} (Fig. 2b and e) and X_{CH_4} (Fig. 2c and f) varying δ_A (the height of the annular chamber) and δ_w (the thickness of the catalyst layer). Comparing Fig. 2a and b or Fig. 2d and e it is evident that η_{int} and, consequently, η_{total} markedly decrease on increasing δ_w. This means that the diffusion limitations in the catalyst pores markedly affect the reactor performances unless the active layer is kept extremely thin (10–15 μm).

Contour lines of η_{total} show a slight negative slope on increasing δ_A in Fig. 2a and d, due to the limitations associated with axial diffusion and gas–solid mass transfer which both increase on widening the annular chamber. Despite, as shown in Table 1, molecular diffusion coefficients in He are about three times greater than those in N_2, both η_{total} and η_{int} are nearly equal with the two carrier gases, especially with small δ_w. This is consistent with previous results obtained by simulating a PdO/Al_2O_3 annular catalytic reactor [4,5] and is due to compensation of limitations associated with gas–solid mass transfer, which are smaller in He than in N_2, and limitations associated with axial diffusion which, inversely, are greater in He than in N_2. Besides η_{int} using N_2 or He as carrier gas are similar because effective diffusion coefficients, which are controlled mainly by Knudsen diffusion in the catalyst, are nearly equal as shown in Table 1.

3. Experimental

A PdO/ZrO_2 (10%, w/w of Pd) catalyst was prepared according to the following procedure. The starting ZrO_2 powders were obtained by calcining

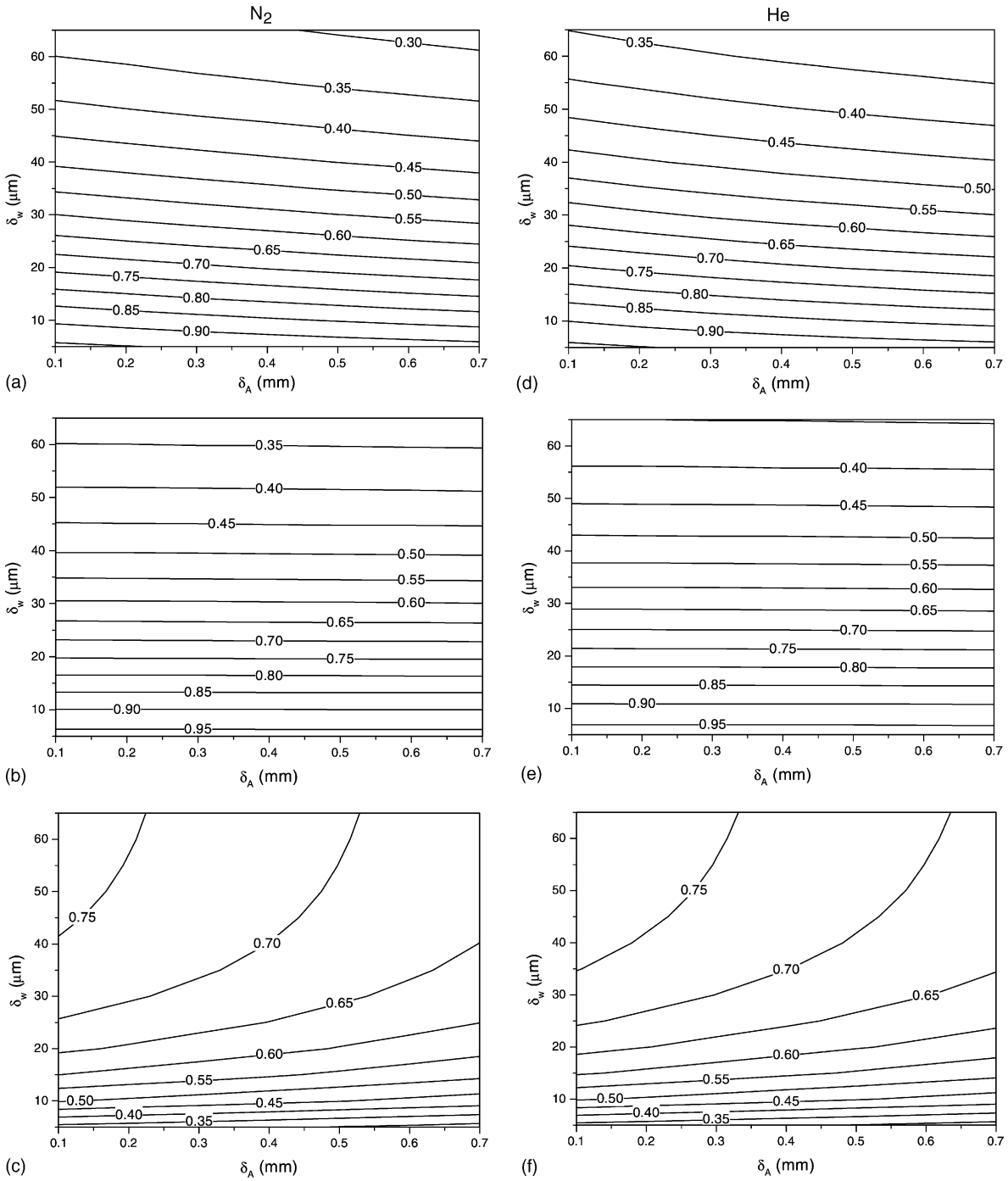

Fig. 2. Simulated contour of (a), (d) η_{total}, (b), (e) η_{int} and (c), (f) X_{CH_4} varying δ_A and δ_w using N_2 or He as carrier gas.

$Zr(OH)_4$ (Mel Chemicals) at 500 °C. The ZrO_2 powders were dry-impregnated with $Pd(NO_3)_2$ aqueous solution (10% Pd, w/w, Aldrich) and then dried at 110 °C for 2 h. The impregnation procedure was repeated several times until Pd metal loading achieved 10% (w/w). The catalyst powder was then calcined at 500 °C in air for 10 h in a muffle furnace. The calcined powder was mixed with HNO_3 solution by ball-milling for 24 h. An α-Al_2O_3 tube (outer radius, $r_i = 3.25$ mm) was wash-coated by dipping into the slurry with a constant withdrawal velocity of 3 cm/min. After flash drying at 280 °C for 5 min, the tube was calcined at 700 °C in a muffle furnace. Then the tube was assembled into the annular reactor mentioned above and was calcined again under air flow (10 cm^3/min at STP) at 800 °C for 10 h. Length, weight and density of the catalyst layer coated on α-Al_2O_3 tube were 10 mm, 6 mg and 2 g/ml, respectively. The catalyst thickness calculated from these data and confirmed by optical microscopy was 15 μm. It is worth noting that the deposition of an adherent layer with controlled thickness and appropriate catalytic and morphological properties is certainly the most demanding task in the construction of the annular reactor. In view of this, although thinner layers could be desirable, the above results were considered satisfactory in view of the indications provided by the model analysis. Further development of the coating technique are currently under development in our labs.

A PdO/γ-Al_2O_3 catalyst was also prepared according to the following procedures described in a previous paper [4]. A submicronic γ-Al_2O_3 powder (Sumitomo, AKP-G015) calcined at 700 °C was dry-impregnated using the same procedure described for the preparation of PdO/ZrO_2. The powder catalyst was mixed with HNO_3 solution by magnetic stirring at 18–20 °C for 10 h. The α-Al_2O_3 tube was wash-coated with the slurry by the same procedures described above. After flash drying at 280 °C for 5 min, the tube was calcined at 700 °C for 10 h in a muffle furnace. The catalyst length, weight and density of the catalyst coated on α-Al_2O_3 were 10 mm, 2 mg and 1.0 g/ml, respectively. The catalyst thickness calculated from these data and confirmed by optical microscopy was 10 μm.

Morphological properties of the catalyst were analyzed by N_2 adsorption/desorption at 77 K (CarloErba Sorptomatic 1900 series) and Hg-porosimetry. PdO/ZrO_2 exhibited a bimodal pore distribution consisting of one mesopore and one macropore family as described above. PdO/γ-Al_2O_3 exhibited a monomodal distribution consisting of mesopores with mean radius and porosity of 9 nm and 0.5225, respectively.

Activity test of CH_4 oxidation over PdO/ZrO_2 and PdO/γ-Al_2O_3 catalysts were performed to collect kinetic data using the annular reactor shown in Fig. 1. Besides $CO + H_2$ oxidation tests were performed over PdO/γ-Al_2O_3 to analyze the thermal behavior of the reactor. Feed gas mixtures with calibrated composition were prepared by mass flow controllers. Reactants and products were analyzed by an on-line GC-TCD (Hewlett Packard, HP6890 Series) equipped with a 5 Å molecular sieve column for separation of O_2, N_2, CH_4 and CO and with a PORAPAK-Q column for separation of CH_4, CO_2 and H_2O. Feed water was injected with a saturator and its concentration was controlled by setting the temperature of a water bath where the saturator was soaked.

Inner radius of the external quartz tube of the annular reactor shown in Fig. 1 was 3.5 mm, whereas outer radius of the α-Al_2O_3 tube was 3.25 mm so to obtain an annular chamber with an average height of 0.25 mm. The bottom of the α-Al_2O_3 tube was stuffed with inorganic binder to prevent gas leakage. Characteristic temperature profiles in the reactor were measured by thermocouple positioned as T.C.1–T.C.3, as shown in Fig. 1.

At standard experimental conditions: feed 0.8% CH_4, 21% O_2, N_2 carrier; pressure = 1 bar; flow rate = 100 cm^3/min at STP, pressure drop was less than 0.1 bar.

4. Results and discussion

4.1. Thermal behavior of the annular reactor

Preliminary to the collection of kinetic data the thermal behavior of the reactor was investigated in order to (i) check the assumption of nearly isothermal behavior and (ii) provide insight on heat dissipation mechanisms. The results are described in the following.

4.1.1. Axial temperature profile in the catalyst layer

First, experiments under operating conditions similar to those adopted in the kinetic tests were

performed. The data were analyzed considering the effect of the overall reaction heat flux calculated by Eq. (13) on the temperature profiles measured over a 10% PdO/γ-Al_2O_3 catalyst:

$$Q_{\text{react}} = F_t y_f X_f (-\Delta H_f) \quad \text{(W)} \tag{13}$$

Overall reaction heat fluxes were (a) 0.30, (b) 0.92 and (c) 1.30 W, respectively. T_1 and T_2 are the axial profiles inside α-Al_2O_3 tube (T.C.1 in Fig. 1) and outside of quartz reactor (T.C.2 in Fig. 1), respectively. T_{1B} is the axial profile inside the tube without the reaction (zero inlet concentration of CH_4). T_1 is supposed to be equal to the catalyst temperature under the reasonable assumption of thermal equilibrium along the cross-section of the ceramic tube. Accordingly $\Delta T_{1\,\text{react}} = T_1 - T_{1B}$ is the temperature increase associated with the reaction, while $\Delta T_{\text{rad}} = T_1 - T_2$ is representative of the temperature gradient in the radial direction.

From inspection of T_{1B} in Fig. 3a–c it was confirmed that, in the absence of reaction, the catalyst was placed just within the isothermal zone of the reactor. According to Fig. 3a the overall reaction heat flux of 0.3 W, which was generated by standard reaction conditions (i.e. CH_4 = 0.8%, O_2 = 21%, flow rate = 100 cm^3/min at STP) with a conversion of 59.8%, did not result in significant temperature increase since $\Delta T_{1\,\text{react}}$ and ΔT_{rad} were less than 6 and 3 °C, respectively. Under such conditions maximum temperature difference along the catalyst bed, $\Delta T_{1\,\text{max}}$ was only 7 °C, i.e. nearly isothermal conditions were achieved.

More demanding conditions with Q_{react} equal to 0.92 W (Fig. 3b) and 1.30 W (Fig. 3c), obtained with 1.92% of CH_4 and 71.8% conversion and with 2.92% of CH_4 and 67.1% conversion, respectively, resulted in consistently higher $\Delta T_{1\,\text{react}}$ as shown by comparison of Fig. 3a with Fig. 3b and c. However $\Delta T_{1\,\text{max}}$ were kept reasonably small at 7 and 9 °C, respectively. Such limited temperature gradients demonstrated that heat dissipation processes in the annular reactor is very effective.

It is worth noting that in most of the experiments of the kinetic study described in the following section the overall reaction heat fluxes were much less than those of the most critical cases discussed above. Therefore it was predicted that the annular reactor would operate under nearly isothermal conditions in all the kinetic tests. Actually, the temperature profiles of T_1 measured during the activity tests confirmed this prediction.

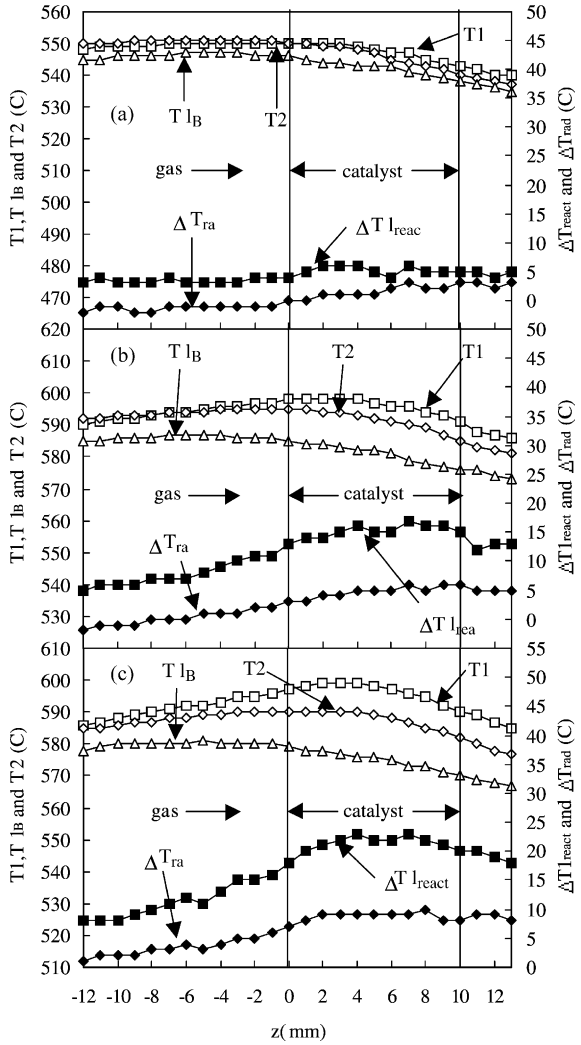

Fig. 3. Temperature profile in the annular reactor during CH_4 combustion tests over PdO/Al_2O_3. (a) Q_{react}: 0.3 W (inlet CH_4: 0.7550%, conversion: 59.8%); $T_{1\,\text{mid}}$: 548 °C. (b) Q_{react}: 0.92 W (inlet CH_4: 1.920%, conversion: 71.80%); $T_{1\,\text{mid}}$: 597 °C. (c) Q_r: 1.30 W (inlet CH_4: 2.921%, conversion: 67.08%); $T_{1\,\text{mid}}$: 548 °C. z = 0 mm: inlet of catalyst bed; z = 10 mm: outlet. Reactant gas flows from right side to left side. Other experimental conditions: gas flow rate, 100 cm^3/min at STP; O_2, 21%; N_2, carrier.

4.1.2. *Mechanism of heat dissipation from the annular reactor*

To provide insight on the mechanism of heat dissipation prevailing in the annular reactor a mixture of

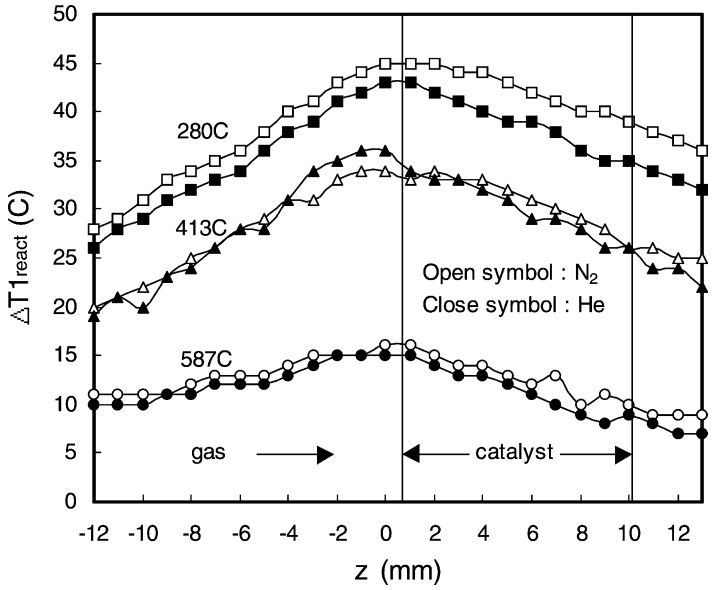

Fig. 4. Temperature increase associated with CO–H_2 combustion over the PdO/γ-Al_2O_3 catalyst at different reaction temperatures. Open symbol: carrier gas N_2; closed symbol: carrier gas He. Inlet composition: 2.75% CO, 5.25% H_2, 21% O_2, N_2 or He balance; conversion: 100%; flow rate: 100 cm^3/min at STP.

CO and H_2 in air (CO = 2.75%, H_2 = 5.25%) was supplied in order to obtain the same overall reaction heat flux, $Q_{\text{react}} = 1.5$ W, at different reaction temperatures. Indeed due to the high reactivity of such a mixture 100% conversion into CO_2 and H_2O could be obtained above 250 °C over PdO/γAl_2O_3 at GHSV = 3×10^6 cm^3/gh at STP.

The effect of reaction temperature on $\Delta T_{1\,\text{react}}$ profiles is shown in Fig. 4. It is evident that $\Delta T_{1\,\text{react}}$ markedly decreases on increasing the reaction temperature at constant overall reaction heat flux, showing that heat dissipation is more effective at high temperature.

In principle there are three mechanisms of heat dissipation, i.e. (i) radiation from catalyst surface to any cold surface in the reactor, (ii) radial heat transfer by convection in the annular gas phase and conduction through the wall of the quartz reactor, and (iii) axial conduction through the wall of the α-Al_2O_3 tube.

The contribution of this latter mechanism can be roughly estimated by

$$Q_{\text{axial}} = A_{\text{axial}} k_{Al_2O_3} \times \left[\frac{T_{1\,\text{mid}} - T_{1\,\text{inlet}}}{L_{\text{up}}} + \frac{T_{1\,\text{mid}} - T_{1\,\text{outlet}}}{L_{\text{down}}} \right] \quad (14)$$

where $T_{1\,\text{mid}}$ is the hot spot temperature and L_{up} and L_{down} the lengths between the hot spot and the inlet and the outlet of the catalytic layer, respectively. Calculations showed that such a contribution is negligible (below 5%) under all the investigated conditions.

In order to collect further information on the role of convective heat transfer, experiments with a reacting mixture using He in place of N_2 as carrier gas were performed. Indeed He should have a marked effect on convective heat transfer under the laminar flow conditions prevailing in the annular chamber since its thermal conductivity is five times higher than that of N_2. Results in Fig. 4 showed that $\Delta T_{1\,\text{react}}$ using He as a carrier gas at 280 °C were lower than those measured using N_2, whereas both at 413 and at 587 °C no effect of the carrier gas was observed. This suggests that convective radial heat transfer is responsible of a significant fraction of dissipated heat at low reaction temperature, whereas at higher temperature, at which heat dissipation is more effective, its role is negligible. As a whole such results confirm previous reports [10,11] indicating radiative heat transfer as the main mechanism of heat dissipation under relevant conditions (high temperature at which kinetic measurements were performed). Indeed radiative heat

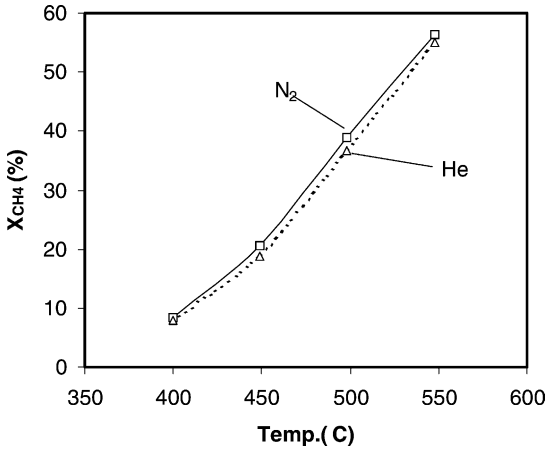

Fig. 5. Effect of carrier gas on CH_4 conversion. Catalyst: PdO/ZrO_2 (10%, w/w of Pd); feed composition: 0.75% CH_4, 20% O_2, carrier gas N_2 or He balance; flow rate: 100 cm^3/min at STP.

transfer increases with the fourth power of temperature and become progressively more effective above 400 °C thanks to the high exposed surface of the catalyst layer.

4.2. Mass transfer limitations

Using the annular reactor coated with PdO/ZrO_2, CH_4 combustion experiments with different carrier gases (N_2 and He) were performed and the results are shown in Fig. 5. In previous investigations [4,5] it was shown that, in the presence of important gas–solid mass transfer limitations, e.g. due to poor mass transfer coefficients associated with annulus eccentricity, the conversions observed with the two carrier gases should be different. As shown in Fig. 5, the difference between the conversions were less than 2%, i.e. within the experimental error. Thus it was concluded that gas–solid mass transfer limitations in the annular reactor used in this research were negligible.

Possible and minimum values of δ_A and δ_w in the actual preparation of Pd/ZrO_2 were 0.25 mm and 15 μm, respectively. For such configuration the results of mathematical model simulations shown in Fig. 2 predict a η_{total} of 0.83 with a conversion of 57.8%. Such a conversion corresponds well to the highest ones observed in the experiments (see Figs. 7–10). Accordingly most of the experimental data collected in the kinetic study reported in the following section were performed under less demanding conditions than the simulated ones. Therefore, we could conclude that the effect of the mass transfer limitations on the reaction rate equation derived in this paper is practically negligible.

4.3. Kinetic analysis on CH_4 combustion over 10% PdO/ZrO_2

Upon establishing the nearly isothermal behavior of the reactor and the scarce impact of mass diffusion limitations an extensive kinetic study on CH_4 combustion was carried out over PdO/ZrO_2 (10%, w/w of Pd). The following ranges of experimental variables were investigated: T = 400–550 °C; GHSV = 10^6 cm^3/gh at STP; feed composition: O_2 = 11.5–21.2%, CH_4 = 0.4–3.2%, H_2O = 0–3.5%, CO_2 = 0–2.7%, N_2 balance. Experiments were performed at atmospheric pressure with negligible pressure drops along the catalyst bed. The maximum investigated temperature was set according to preliminary tests performed on powder catalysts showing significant deactivation at temperatures above 550 °C, particularly in the presence of water in the feed. Under the investigated conditions activity, as determined by repeated standard tests (O_2 = 21.2%, CH_4 = 0.8%, H_2O = 0–3.5%, N_2 balance; T = 400, 450, 500, 550 °C), was observed constant for over 50 h.

4.3.1. Effect of reactants and products on the reaction rate

As shown in Fig. 6, the conversion vs reaction temperature curve with 11.5% O_2 practically overlaps that obtained with 21.2% O_2. The absence of any effect of O_2 concentration on reaction rate under the very lean conditions considered in this paper is in good agreement with several literature investigations [4,5,7,9,12] reporting approximately zeroth order dependence on O_2 concentration of CH_4 combustion rate.

On the other hand, conversion markedly decreased on increasing H_2O concentration in the feed, as shown in Fig. 7. Such conversion decrease was due to inhibition and not to deactivation since original activity was reversibly restored under standard H_2O free conditions. H_2O inhibition was reported by several authors in the literature [4,5,7–9,13]. However, the data herein reported demonstrated that H_2O inhibits the reaction up to 550 °C, which is a significantly higher

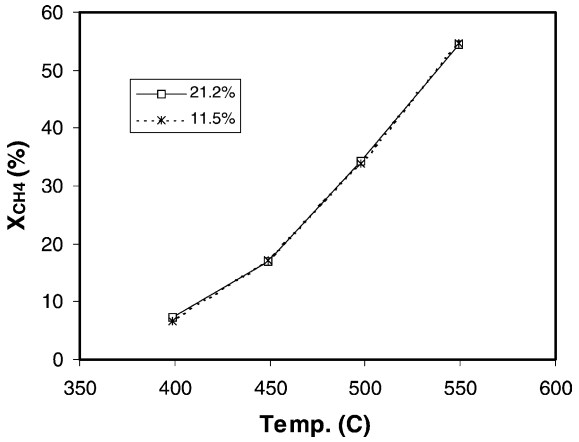

Fig. 6. Effect of O_2 concentration.

temperature than those investigated in most of the paper cited above. Ciuparu et al. [14,15] recently reported that, during CH_4 combustion over a PdO/ZrO_2 (3%, w/w of Pd) catalyst, water inhibition was observed up to 600 °C. However conversion data were collected under transient temperature programmed conditions which, as suggested in the paper, could bias the true temperature effect on H_2O inhibition due to delay in equilibration of adsorbed H_2O. In the present work conversion data were collected by repeating four GC analyses at each constant temperature in a time interval of more than 1 h. Accordingly our evidences indicate that H_2O inhibition is important at high temperature even at steady state conditions. This is partly in line with the results described in a previous paper [4,5] which indicated a strong H_2O inhibition effect over a γ-Al_2O_3 supported PdO catalyst up to 600 °C. On the other hand the kinetic data collected in this work show a H_2O reaction order equal to −0.32 which is significantly higher than the values −0.8 to −1 reported in most of the literature studies [7–9]. Such a difference may be partly ascribed to the higher temperature range at which the data were herein collected [13–15]. However an effect of the support is also evident when comparing the behavior of PdO/ZrO_2 with that observed over a PdO/γ-Al_2O_3 catalyst [4,5] in the same temperature range. Over PdO/ZrO_2, inhibition seems to rapidly approach saturation between 1 and 3% of H_2O in the feed depending on reaction temperature, whereas over PdO/γ-Al_2O_3 a gradual conversion decrease was observed up to 10% H_2O in the feed which corresponded to a negative reaction order of about −0.5.

H_2O inhibition has been ascribed either to reversible adsorption over single PdO [8,16] sites

$$PdO + H_2O \Leftrightarrow Pd(OH)_2$$

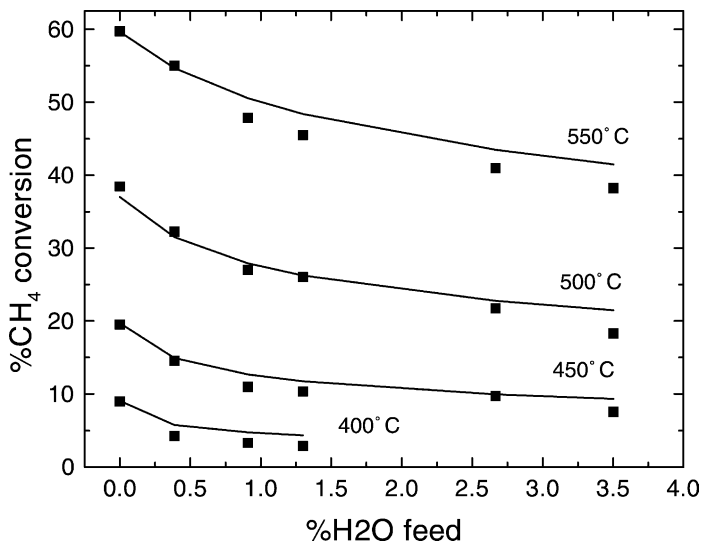

Fig. 7. Effect of H_2O concentration. Dots: experimental data. Lines: model fitting with Eq. (15) and parameters of Table 2.

or to dissociative adsorption onto a pair of oxidized and reduced sites [7]

$$H_2O + {}^* + O^* \Leftrightarrow 2OH^*$$

Ribeiro et al. [8] commented that reversible formation of $Pd(OH)_2$, could be responsible of H_2O inhibition at low temperature based on the report that $Pd(OH)_2$ decomposition started from 250 °C [17]. Burch et al. [13] reported that H_2O inhibition was still effective up to 400 °C, suggesting that this could be due to stabilization of $Pd(OH)_2$ by the support material at temperatures higher than 250 °C. They also reported that the inhibition disappeared above 450 °C. However under the experimental conditions adopted in their investigation such an indication could be biased both by the onset of internal diffusion limitations (particle size of 250–600 μm, was not small enough to prevent effects of mass transfer limitations) and by saturation of conversion which at 450 °C reached values close to 100%. According to TPD analysis with Pd/Al_2O_3 [18] desorption of H_2O started from 230 °C, but significant H_2O release was observed up to 750 °C. This suggest that some H_2O adsorbed on the support and/or palladium still persist at high temperature which may affect the catalytic performances of the system. Concerning the role of the support it has been reported in a recent paper [19] that FTIR experiments demonstrated that dehydroxilation of the PdO surface is faster in the presence of high oxygen mobility supports such as ZrO_2. This is consistent with the milder H_2O inhibition herein observed.

As shown in Fig. 8, CO_2 was found to inhibit CH_4 combustion rate up to 550 °C similar to H_2O. In fact a significant conversion decrease was observed with limited CO_2 concentration (up to 1.3%) in the feed, whereas inhibition effect apparently reached saturation at higher CO_2 concentration. Literature reports on CO_2 inhibition are quite controversial. Over a $PdO/\gamma\text{-}Al_2O_3$ catalyst van Giezen et al. [9] did not found any inhibition effect up to 5% CO_2 in the feed and up to 500 °C. This was in line with early reports by Cullis et al. [16] for palladium supported over different oxides. On a similar $PdO/\gamma\text{-}Al_2O_3$ Burch et al. [13] reported a very weak inhibition effect in the presence of 20% CO_2 which completely disappeared when water was added to the feed. On the other hand for a PdO catalyst supported onto Al_2O_3 stabilized with SiO_2, Ribeiro et al. [8] reported a negative reaction order of −2 at 280 °C, which however was evident only at CO_2 concentration higher than 0.5%. Similarly Fujimoto et al. [7] reported a −2 reaction order at 280 °C over a PdO/ZrO_2 catalyst which was observed only for CO_2 above 3–5%. Fujimoto et al. suggested that at low CO_2 concentration inhibition was masked by

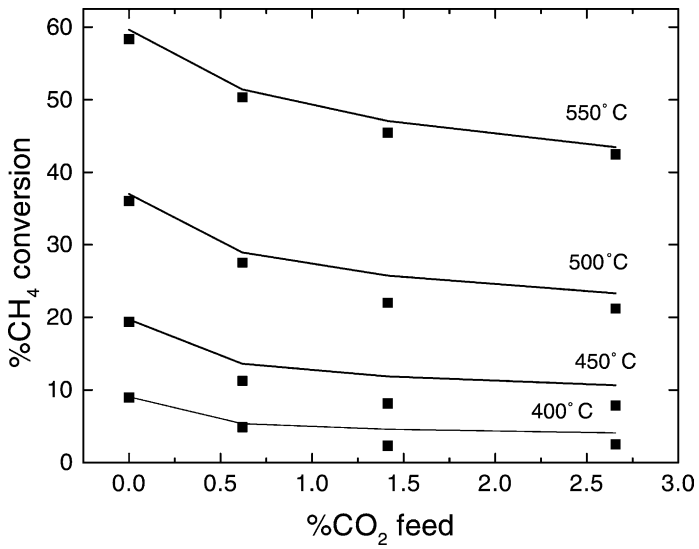

Fig. 8. Effect of CO_2 concentration. Dots: experimental data. Lines: model fitting with Eq. (15) and parameters of Table 2.

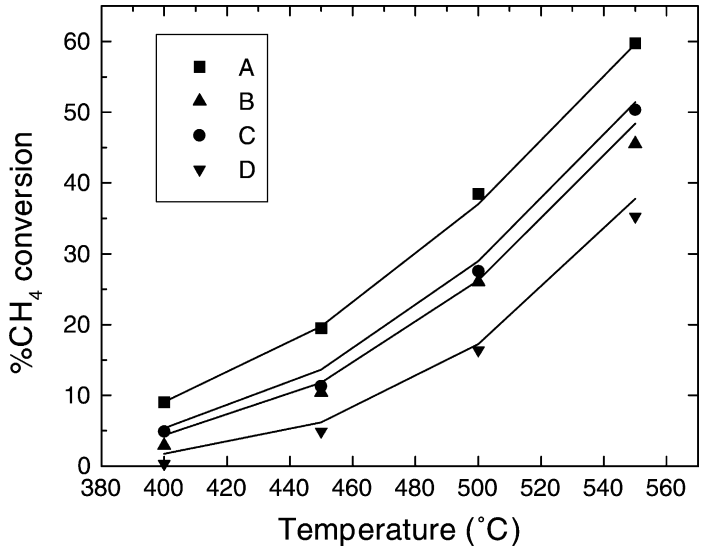

Fig. 9. Combined effects of H_2O and CO_2: (A) without H_2O and CO_2; (B) H_2O (1.3%); (C) CO_2 (0.6%); (D) H_2O (1.3%) + CO_2 (0.6%). Dots: experimental data. Lines: model fitting with Eq. (15) and parameters of Table 2.

H_2O which compete for adsorption onto the same active sites. A similar explanation was also provided by Burch et al. [13].

Such discrepancies may arise from a strong role of the support in the inhibition chemistry as suggested also by Burch et al. (1995) who observed a large difference of sensitivity to CO_2 when comparing an Al_2O_3 with a SiO_2 supported PdO catalyst, the latter being much more affected by CO_2. In this work the role of the support was confirmed by investigating CO_2 inhibition over a PdO/γ-Al_2O_3 catalyst within the annular reactor under very similar operating conditions to those adopted for PdO/ZrO_2. At 510 °C no inhibition was observed up to 10% CO_2. Therefore, it was clear that the nature of support material could affect the extent of the inhibition by CO_2, although the surface chemistry of the process has not been clarified yet.

In addition to the role of the support, the effect of the reaction temperature could be considered to explain the difference of the data collected herein, showing similar inhibition effect of CO_2 and H_2O in a temperature range from 400 to 550 °C, from those collected in literature works reporting that at lower temperature of 280–400 °C the effect of CO_2 is masked by the presence of H_2O (either in the feed or as a reaction product) which was supposed to displace adsorbed CO_2. To definitely rule out this possibility experiments with both H_2O and CO_2 in the feed were performed. As shown in Fig. 9, conversions obtained in such experiments were significantly lower than those achieved with the same amount of H_2O and CO_2 when separately fed, indicating that the inhibition effects of H_2O and CO_2 were not reciprocally masked but co-operate under the investigated conditions. Such a result may be consistent with the relatively small negative H_2O reaction order obtained in this work suggesting that over the investigated ZrO_2 supported catalyst and under the actual operating conditions active site occupancy of adsorbed water is relatively small.

The effect of CH_4 concentration was also investigated. Results in Fig. 10 show a conversion decrease on increasing CH_4 concentration which, under the integral conversion conditions obtained in the present work, can be associated to the larger amount of inhibiting products obtained from the reaction.

4.3.2. Data fitting with a power law expression

A simple power law expression has been attempted to fit the experimental data described above:

$$r = k_r P_{CH_4}^{\alpha} P_{H_2O}^{\beta} P_{CO_2}^{\gamma} \quad (15)$$

Zeroth order in O_2 concentration was assumed according to the experimental results. Besides CH_4 reaction order, α, was fixed equal to 1 in line with several liter-

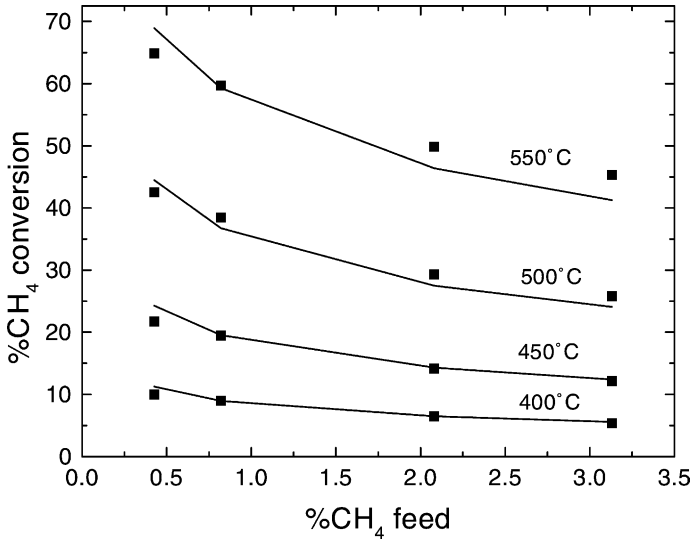

Fig. 10. Effect of CH_4 concentration. Dots: experimental data. Lines: model fitting with Eq. (15) and parameters of Table 2.

ature indications [4,5,7–9,12]. The reactor was modeled as an integral, pseudo-homogeneous, isothermal PFR in view of the results on the negligible impact of diffusion limitations described in the previous sections. Model fittings of the experimental data with the parameter estimates reported in Table 2 are plotted in Figs. 7, 8 and 10 (solid lines). The overall agreement was satisfactory although statistical *F*-test was not accomplished. Small negative reaction order were obtained for both H_2O and CO_2 as discussed in the previous section. An apparent activation energy of 108 kJ/mol was estimated which is slightly lower than those reported in the literature when product inhibition effects are taken into account [9]. This difference is consistent with the reaction order of H_2O and CO_2 which are significantly lower than those reported in other literature studies which suggest a lower importance of the adsorption terms on apparent activation energy with respect to that prevailing in kinetic studies performed at lower temperatures.

Table 2
Estimated values of kinetic parameters in rate equation (15)

$r = k_r P_{CH_4} P_{H_2O}^{\beta} P_{CO_2}^{\gamma}$ (mol/kg$_{cat}$ s)
k_r at 673 K $= 2.22 \times 10^{-2}$ mol/kg$_{cat}$/s/bar$^{0.43}$
$E_{att} = 108$ kJ/mol
$\beta = -0.32$
$\gamma = -0.25$

5. Conclusions

By means of a specifically designed annular reactor the kinetics of CH_4 combustion over PdO/ZrO_2 under O_2 rich condition, was investigated in a higher temperature range (400–550 °C) than those usually considered in literature studies.

Theoretical investigation by means of mathematical modeling showed that the impact of diffusional limitations on kinetic measurements under the actual high temperature conditions was negligible. Experimental tests performed using He and N_2 as carrier gas provided the same conversion level confirming the negligible role of external diffusion.

Experiments addressing the thermal behavior of the reactor demonstrated the ability to obtain nearly isothermal conditions also with high conversion (60%) and high CH_4 inlet concentration (3%), mainly due to effective dissipation of reaction heat by radiation.

The results of the kinetic study indicated that under the investigated conditions both H_2O and CO_2 similarly inhibit the reaction rate up to 550 °C. Indications

on a primary role of the support on the extent of both such inhibition effects were found.

Acknowledgements

Financial support for this work has been provided by MIUR Rome, Italy, and by Japan Cooperation Center Petroleum Tokyo, Japan.

References

[1] P. Forzatti, G. Groppi, Catal. Today 54 (1999) 49.
[2] R.B. Anderson, K.C. Stein, J.J. Feenan, L.J.E. Hofer, Ind. Eng. Chem. 53 (1961) 809.
[3] J.G. McCarty, Catal. Today 26 (1995) 283.
[4] G. Groppi, W. Ibashi, M. Valentini, P. Forzatti, Chem. Eng. Sci. 56 (2001) 831.
[5] G. Groppi, W. Ibashi, E. Tronconi, P. Forzatti, Chem. Eng. J. 82 (2001) 57.
[6] R.A. Dalla Betta, K. Tsurumi, T. Shoji, R.L. Garten, US Patent 5 405 260 (April 11, 1995).
[7] K. Fujimoto, F.H. Ribeiro, M. Avalos-Borja, E. Iglesia, J. Catal. 179 (1998) 431.
[8] F.H. Ribeiro, M. Chow, R.A. Dalla Betta, J. Catal. 146 (1994) 537.
[9] C. van Giezen, F.R. van den Berg, J.L. Kleinen, A.J. van Dillen, J.W. Geus, Catal. Today 47 (1999) 287.
[10] A. Beretta, P. Baiardi, D. Prina, P. Forzatti, Chem. Eng. Sci. 54 (1999) 765.
[11] A. Beretta, G. Groppi, L. Majocchi, P. Forzatti, Appl. Catal. A 187 (1999) 49.
[12] Y.Y. Yao, Ind. Eng. Prod. Res. Dev. 19 (1980) 293.
[13] R. Burch, F.J. Urbano, P.K. Loader, Appl. Catal. A 123 (1995) 173.
[14] D. Ciuparu, N. Katsikis, L. Pfefferle, Appl. Catal. A 216 (2001) 209.
[15] D. Ciuparu, L. Pfefferle, Appl. Catal. A 209 (2001) 415.
[16] C.F. Cullis, T.G. Nevell, D.L. Trimm, J. Chem. Soc., Faraday Trans. 1 (1972).
[17] R.J. Card, J.L. Schmitt, J.M. Simpson, J. Catal. 79 (1983) 13.
[18] D.L. Mowery, M.S. Graboski, T.R. Ohno, R.L. McCormick, Appl. Catal. B 21 (1999) 157.
[19] D. Ciuparu, M.R. Lyubovrky, E. Altman, L.D. Pfefferle, A. Datye, Cat. Rev. Sci. Eng. 44 (2002) 593.